Title	Performance of parametric spectro-temporal analyzer (PASTA)
Author(s)	Zhang, C; Wei, X; Wong, KKY
Citation	Optics Express, 2013, v. 21 n. 26, p. 32111-32122
Issued Date	2013
URL	http://hdl.handle.net/10722/202822
Rights	Optics Express. Copyright © Optical Society of America.

Performance of parametric spectro-temporal analyzer (PASTA)

Chi Zhang, Xiaoming Wei, and Kenneth K. Y. Wong[*]

Photonic Systems Research Laboratory, Department of Electrical and Electronic Engineering, The University of Hong Kong, Pokfulam Road, Hong Kong
[*]*kywong@eee.hku.hk*

Abstract: Parametric spectro-temporal analyzer (PASTA) is an entirely new wavelength resolving modality that focuses the spectral information on the temporal axis, enables ultrafast frame rate, and provides comparable resolution and sensitivity to the state-of-art optical spectrum analyzer (OSA). Generally, spectroscopy relies on the allocation of the spectrum onto the spatial or temporal domain, and the Czerny-Turner monochromator based conventional OSA realizes the spatial allocation by a dispersive grating, while the mechanical rotation limits its operation speed. On the other hand, the PASTA system performs the spectroscopy function by a time-lens focusing mechanism, which all-optically maps the spectral information on the temporal axis, and realizes the single-shot spectrum acquisition. Therefore, the PASTA system provides orders of magnitude improvement on the frame rate, as high as megahertz or even gigahertz in principle. In addition to the implementation of the PASTA system, in this paper, we will primarily discuss its performance, including the tradeoff between the frame rate and the wavelength range, factors that affect the wavelength resolution, the conversion efficiency, the power saturation and the polarization sensitivity. Detection bandwidth and high-order dispersion introduced limitations are also under investigation. All these analyses not only provide an overall guideline for the PASTA design, but also help future research in improving and optimizing this new spectrum resolving technology.

References and links

1. D. A. Skoog, F. J. Holler, and S. R. Crouch, *Principles of Instrumental Analysis*, 6th ed. (Thomson Brooks/Cole, 2007).
2. D. Derickson, ed., *Fiber Optic, Test and Measurement* (Prentice Hall, 1998).
3. M. Czerny and A. F. Turner, "Uber den Astigmatismus bei Spiegelspektrometern," Z. Phys. **61**(11–12), 792–797 (1930).
4. A. B. Shafer, L. R. Megill, and L. A. Droppleman, "Optimization of the Czerny–Turner spectrometer," J. Opt. Soc. Am. **54**(7), 879–887 (1964).
5. B. R. Biedermann, W. Wieser, C. M. Eigenwillig, T. Klein, and R. Huber, "Direct measurement of the instantaneous linewidth of rapidly wavelength-swept lasers," Opt. Lett. **35**(22), 3733–3735 (2010).
6. C. Zhang, K. K. Y. Cheung, P. C. Chui, K. K. Tsia, and K. K. Y. Wong, "Fast swept-source generation based on fiber optical parametric amplifier," in *Conference on Lasers and Electro-Optics* (2011).
7. H. A. Haus, "Mode-locking of lasers," IEEE J. Sel. Top. Quantum Electron. **6**(6), 1173–1185 (2000).
8. L. N. Binh and N. Q. Ngo, *Ultra-Fast Fiber Lasers: Principles and Applications with MATLAB® Models* (CRC Press, 2011).
9. I. V. Rubtsov, R. M. Russo, T. Albers, P. Deria, D. E. Luzzi, and M. J. Therien, "Visible and near-infrared excited-state dynamics of single-walled carbon nanotubes," Appl. Phys. A Mater. Sci. Process. **79**(7), 1747–1751 (2004).
10. J. Chou, O. Boyraz, D. Solli, and B. Jalali, "Femtosecond real-time single-shot digitizer," Appl. Phys. Lett. **91**(16), 161105 (2007).
11. D. R. Solli, J. Chou, and B. Jalali, "Amplified wavelength-time transformation for real-time spectroscopy," Nat. Photonics **2**(1), 48–51 (2008).

12. J. Chou, D. R. Solli, and B. Jalali, "Real-time spectroscopy with subgigahertz resolution using amplified dispersive Fourier transformation," Appl. Phys. Lett. **92**(11), 111102 (2008).
13. K. Goda, D. R. Solli, K. K. Tsia, and B. Jalali, "Theory of amplified dispersive Fourier transformation," Phys. Rev. A **80**(4), 043821 (2009).
14. G. P. Agrawal, *Fiber Optic Communication Systems*, 3rd ed. (Wiley-Interscience, 2002).
15. http://tmi.yokogawa.com/products/optical-measuring-instruments/optical-spectrum-analyzer/aq6370c-optical-spectrum-analyzer/.
16. J. W. Goodman, *Introduction To Fourier Optics*, 3rd ed. (Roberts and Company, 2005).
17. B. H. Kolner, "Space-time duality and the theory of temporal imaging," IEEE J. Quantum Electron. **30**(8), 1951–1963 (1994).
18. M. T. Kauffman, W. C. Banyai, A. A. Godil, and D. M. Bloom, "Time-to-frequency converter for measuring picosecond optical pulses," Appl. Phys. Lett. **64**(3), 270–272 (1994).
19. C. Zhang, J. Xu, P. C. Chui, and K. K. Y. Wong, "Parametric Spectro-Temporal Analyzer (PASTA) for real-time optical spectrum observation," Sci. Rep. **3**, 2064 (2013).
20. M. A. Foster, R. Salem, D. F. Geraghty, A. C. Turner-Foster, M. Lipson, and A. L. Gaeta, "Silicon-chip-based ultrafast optical oscilloscope," Nature **456**(7218), 81–84 (2008).
21. C. Zhang, K. K. Y. Cheung, P. C. Chui, K. K. Tsia, and K. K. Y. Wong, "Fiber optical parametric amplifier with high-speed swept pump," IEEE Photonics Technol. Lett. **23**(14), 1022–1024 (2011).
22. C. V. Bennett and B. H. Kolner, "Aberrations in temporal imaging," IEEE J. Quantum Electron. **37**(1), 20–32 (2001).
23. C. Zhang, P. C. Chui, and K. K. Y. Wong, "Comparison of the state-of-art phase modulators and parametric mixers in time-lens applications under different repetition rates," accepted by Applied Optics (available online).
24. M. E. Marhic, K. K. Y. Wong, and L. G. Kazovsky, "Wide-Band tuning of the gain spectra of one-pump fiber optical parametric amplifiers," IEEE J. Sel. Top. Quantum Electron. **10**(5), 1133–1141 (2004).
25. C. V. Bennett and B. H. Kolner, "Principles of parametric temporal imaging—Part I: System configurations," IEEE J. Quantum Electron. **36**(4), 430–437 (2000).
26. C. V. Bennett and B. H. Kolner, "Principles of parametric temporal imaging—Part II: System performance," IEEE J. Quantum Electron. **36**(6), 649–655 (2000).
27. N. Yoshizawa and T. Imai, "Stimulated Brillouin scattering suppression by means of applying strain distribution to fiber with cabling," J. Lightwave Technol. **11**(10), 1518–1522 (1993).
28. K. K. Y. Wong, M. E. Marhic, K. Uesaka, and L. G. Kazovsky, "Polarization-independent one-pump fiber optical parametric amplifier," IEEE Photonics Technol. Lett. **14**(11), 1506–1508 (2002).

1. Introduction

Optical power detection as a function of wavelength is one of the most essential measurement techniques in photonic systems [1,2]. Conventional optical spectrum analyzer (OSA) is widely accepted in both industries and laboratories, owing to its fine accuracy and wide detection range. Most of the OSA systems are based on the mechanical scanning of a dispersive element within a monochromator, which transmits a selectable narrow band of wavelengths from a wider range available at the input [3]. The rotation of the dispersive element directs different bands of wavelength sequentially to the exit slit, which will filter out a single wavelength and block the rest [4]. However, this mechanical scanning limits its acquisition speed; it is quite slow and usually operates in several frames per second, almost impossible for ultrafast applications. To enhance its operation speed, the exit slit can be replaced by a linear CCD sensor. Therefore, no mechanical rotation is required, and operation speed will be greatly enhanced, e.g. up to 1 MHz. However, it also experiences poor resolution and detection sensitivity. In particular, real-time spectroscopy has been of great importance to analyze some dynamical processes, especially non-repetitive transient phenomena, including (i) the instantaneous linewidth measurement of swept-source [5,6], (ii) the spectrum evolution of a laser cavity during its stabilizing process [7,8], and (iii) the chemical dynamics [9], etc.

Fortunately, the concept of single-shot measurement makes this ultrafast operation possible, which means we can obtain a complete spectrum from single frame information [10–12]. By means of the group-velocity dispersion (GVD), which introduces temporal delay between different wavelengths, therefore the spectral information will be all-optically encoded on the temporal axis (wavelength-to-time mapping) [13]. Therefore, a real-time spectroscopy named amplified dispersive Fourier transformation (ADFT) has achieved the frame rate of 25 MHz [11]. While for the monochromator based OSA system, there are two stages of mapping, it first maps the wavelength into spatial position, and then uses the mechanical scanning to map the spatial position into time. The latter mechanical scanning

largely limits the operating speed of OSA, while the GVD based wavelength-to-time mapping enables much faster speed.

On the other hand, when we discuss about the accuracy of spectroscopy, it usually emphasizes on the resolution and the detection sensitivity. However, the ultrafast operation will greatly compromise the detection sensitivity. In particular, the challenges remain at the photodetector owing to the tradeoff between its bandwidth and sensitivity [14]. Large bandwidth photodetector usually has worse detection sensitivity. Nevertheless, although the conventional OSA system is not energy efficient, by operating slowly and within a small bandwidth, it accumulates enough energy over extended period of time (e.g. 200 ms) to achieve very high detection sensitivity (e.g. –90 dBm according to the Yokogawa AQ6370 series [15]). Large detection bandwidth is required in the GVD based wavelength-to-time mapping, owing to its fast operating speed. Moreover, the ADFT detectable power would be quite low because of the inherent fiber insertion loss along the dispersive stretching process. Therefore, it is commonly amplified by a Raman amplifier [13]. Since this dispersive stretching is an energy diverging process, if we can reverse it to an energy converging process, the detection sensitivity will be greatly enhanced. Similar to the space-lens focusing mechanism, where parallel light beams with different angles would focus at different positions at the focal plane [16], and based on the space-time duality, the time-lens could focus the same wavelength at a single temporal point, as shown in Fig. 1(b) [17,18].

In addition to the detection sensitivity, resolution is also of great importance in real-time spectroscopy. Compared with the ADFT based spectroscopy under the same output dispersion, the time-lens focusing mechanism not only provides the wavelength-to-time mapping with finer resolution, but also covers a wider range of initial input conditions; namely, the input signal can be an arbitrary waveform within the time-lens effective range, rather than a short pulse waveform required by the ADFT, as shown in Fig. 1. When this dispersion process is incorporated with a time-lens as in the time-lens focusing mechanism, the same wavelength distributed over the input time span can focus on a single time point, and much wider range of initial input conditions can be accommodated. Moreover, each single wavelength would experience an energy converging process in PASTA, and better detection sensitivity and resolution can be obtained under the same output dispersion.
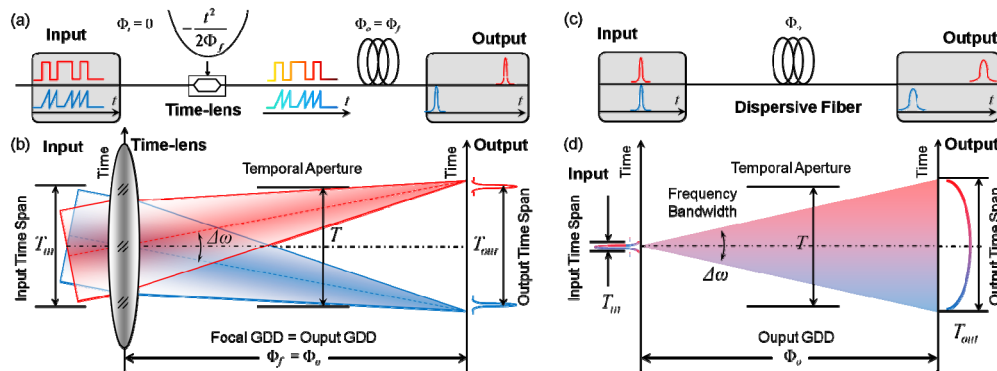

Fig. 1. Principle of the time-lens focusing mechanism, compared with the ADFT mechanism. (a) Schematic diagram shows the relative temporal position between two wavelengths across the PASTA system; (b) calculated temporal ray diagram of the time-lens focusing, illustrates the temporal transformation of two wavelengths along the system, and how they are separated and focused on the focal plane; (c) and (d) corresponding schematic and temporal ray diagrams of the ADFT mechanism.

Based on the time-lens focusing mechanism, we recently developed an entirely new ultrafast wavelength resolving modality called parametric spectro-temporal analyzer (PASTA) [19]. The dispersion-induced wavelength-to-time mapping overcomes the speed limitation, and the time-lens focusing helps achieving better detection sensitivity and resolution, and operating under a wide range of initial input conditions. The dispersion

configurations decide the PASTA performance; here larger dispersion can achieve finer spectral resolution [19]. It is noted that, Fourier transform is one of the most remarkable properties of a converging lens, and in a previous work about ultrafast optical oscilloscope [20], which was in the opposite direction from our current work since it leveraged the spectral information to retrieve sharp temporal resolution, so small dispersion was employed. In this paper, we present an analysis of PASTA performance in different aspects, including the resolution, the wavelength range, the conversion efficiency, and the power saturation in this wideband time-lens focusing mechanism. We will discuss in the subsequent parts.

2. Working principles

In order to realize the ultrafast spectro-temporal analysis, it is required to have the single-shot imaging [10,11], which directly allocates the spectral information in the temporal axis. Although this wavelength-to-time mapping can be achieved by pure dispersion, it is inevitably limited by the initial temporal distribution, and initial temporal spacing will blur the output mapping relation. In view of this constraint, it is illustrative to review the concept of the converging lens and the space-time duality relation in the context of designing a PASTA system.

Table 1. Analogous Quantities between the Space-lens and Time-lens System

Space-lens	Time-lens
Spatial pupil size	Temporal aperture
Spatial angle	Temporal wavelength (or frequency)
Spatial distance	Temporal group-delay dispersion (GDD)
Focal length	Focal group-delay dispersion (GDD)
Parallel beam	Single wavelength

The space-time duality is based on the analogy between the paraxial diffraction in spatial domain, and narrow-band dispersion in temporal domain [17]. Accordingly, we can identify some analogous pairs between the space-lens and time-lens system, as shown in Table 1. Moreover, there are also several analogous processes, e.g. the focusing mechanism. In spatial optics, when a parallel light beam passes through a converging lens, it will focus at one spatial position at the focal plane, as long as it illuminates within the pupil size. According to the space-time duality, we can also perform this mechanism in temporal domain. The parallel light beam corresponds to a single wavelength such as a continuous-wave (CW) source; while the beam size corresponds to the temporal aperture, and the spatial output distribution corresponds to the intensity variation over time. Therefore, when a single wavelength CW source passes through a time-lens, it will be focused at one temporal point at the focal plane (i.e. output GDD equals focal GDD), as long as it can be collected by the temporal aperture of the time-lens. Figure 1(a) shows the schematic diagram of the time-lens focusing mechanism, and in Fig. 1(b), the temporal ray diagram describes this mechanism in the form of the space-lens. To simplify the derivations, we assume the input signal $E_s(t)$ is a CW source at the wavelength of λ_0, and the temporal aperture of the time-lens is T, then its electric field can be expressed as:

$$E_s(t) = \sqrt{I_s} \times \mathrm{rect}\left(\frac{t}{T}\right) \times \exp\left(i2\pi \frac{c}{\lambda_0} t\right) \tag{1}$$

where I_s is the signal intensity, and its Fourier transform is as follows:

$$\overline{E}_s(\omega) = \sqrt{\frac{I_s}{2\pi}} \cdot T \, \mathrm{sinc}\left[\frac{T}{2\pi}\left(\omega - \frac{2\pi c}{\lambda_0}\right)\right] \tag{2}$$

Assuming an ideal time-lens is realized by introducing quadratic phase modulation in temporal domain: $t_f(t) = \exp(-it^2/2\Phi_f)$, where Φ_f is the focal GDD. After the time-lens, the optical field becomes:

$$E_s'(t) = E_s(t)t_f(t) \tag{3}$$

Here, its Fourier transform takes the form of $\overline{E}_s'(\omega)$ in the frequency domain. Then, the linear swept frequency is realigned by a spool of dispersive fiber, with the output GDD $\Phi_o = \beta_{2o}L_o$, and it adds a quadratic phase modulation in the frequency domain: $G_o(\omega) = \exp(-i\Phi_o\omega^2/2)$. Therefore, the output field becomes:

$$
\begin{aligned}
E_o(t) &= \mathcal{F}^{-1}\left\{\overline{E}_s'(\omega)\cdot G_o(\omega)\right\} \\
&= \frac{1}{2\pi}\int_{-\infty}^{+\infty}\left[\int_{-\infty}^{+\infty}E_s(t')t_f(t')\exp(-i\omega t')dt'\right]G_o(\omega)\exp(i\omega t)d\omega \\
&= \int_{-\infty}^{+\infty}g_o(t-t')E_s(t')t_f(t')dt' \\
&= \sqrt{I_s}g_o(t)\int_{-\infty}^{+\infty}\exp\left[i\left(\frac{1}{\Phi_o}-\frac{1}{\Phi_f}\right)\frac{t'^2}{2}\right]E_s(t')\exp\left(-i\frac{t}{\Phi_o}t'\right)dt'
\end{aligned}
\tag{4}
$$

where $g_o(t) = (2\pi i\Phi_o)^{-1/2}\exp(it^2/2\Phi_o)$ is the inverse Fourier transform of the frequency phase shift $G_o(\omega)$, introduced by the output dispersion. At the focal plane, namely $\Phi_o = \Phi_f$, we can obtain the output field in a simplified form:

$$E_o(t) = g_o(t)\overline{E}_s\left(\frac{t}{\Phi_o}\right) \tag{5}$$

Substituting Eq. (2) and $g_o(t)$ into Eq. (5), the output field can be expressed as:

$$E_o(t) = \frac{1}{\sqrt{2\pi i\Phi_o}}\exp\left(i\frac{t^2}{2\Phi_o}\right)\sqrt{\frac{I_s}{2\pi}}\cdot T\,\mathrm{sinc}\left[\frac{T}{2\pi\Phi_f}\left(t-\frac{2\pi c}{\lambda_0}\Phi_f\right)\right] \tag{6}$$

Therefore, we can obtain the intensity trace with the phase term is dropped:

$$I(t) = |E_o(t)|^2 = \frac{I_s T^2}{4\pi^2|\Phi_o|}\mathrm{sinc}^2\left[\frac{T}{2\pi\Phi_f}\left(t-\frac{2\pi c}{\lambda_0}\Phi_f\right)\right] \tag{7}$$

From Eq. (7), it is easy to obtain the wavelength-to-time relation:

$$t = \frac{2\pi c\Phi_f}{\lambda_0} = \omega_0\Phi_f \tag{8}$$

It can be observed that the time is inversely proportional to wavelength λ_0, and proportional to frequency ω_0. By differentiating both sides of Eq. (8), the mapping step can be shown as:

$$\Delta t = \frac{2\pi c\Phi_f}{\lambda_0^2}\Delta\lambda \tag{9}$$

Equations (8) and (9) are the basis of the time-lens focusing mechanism applied in the PASTA system.

3. Experimental setup and results

Figure 2 illustrates the detailed experimental setup of PASTA system, which mainly consists of two parts, the time-lens and the output dispersion. First, the input signal passes through the parametric mixing time-lens, which is implemented by two-stage four-wave mixing (FWM).

In the first-stage FWM, the signal was combined with a swept pump [21]. A 10-GHz mode-lock fiber laser generated 4-ps short pulses at the wavelength of 1555 nm, and its repetition rate was down-converted to 100 MHz by an amplitude modulator (AM). Since the fiber Bragg grating (FBG2) was centered at the pump wavelength, the pump pulse was stretched by forward and backward passing through the 16.3-km dispersion-compensating fiber (DCF). Since the pump GDD is defined as $\Phi_p = \beta_{2p}L_p$, here it is required that the focal GDD $\Phi_f = \Phi_p/2 = \beta_{2p}L_p/2$, should be equal to the output GDD $\Phi_o = \beta_{2o}L_o$. However, even though $L_p = 2L_o$, β_{2p} is larger than β_{2o}, owing to the dispersion slope. Therefore, another spool of 13.1-km single-mode fiber (SMF) was added in the pump branch to ensure $\Phi_f = \Phi_o$ (detailed matching relation is shown in Fig. 3). This swept pump, as well as the input signal, were coupled into a 150-m highly-nonlinear dispersion-shifted fiber (HNL-DSF1), with zero-dispersion wavelength (ZDW) at 1554 nm, and generated the idler with doubled swept range of the pump. The second-stage FWM was pumped by a CW source, and its wavelength was aligned with the first-stage swept-pump at 1555 nm. Combined with the first-stage idler, the CW pump was launched into another 50-m HNL-DSF2 (with the same ZDW), and we can achieve the quadratic phase modulation on the input signal.
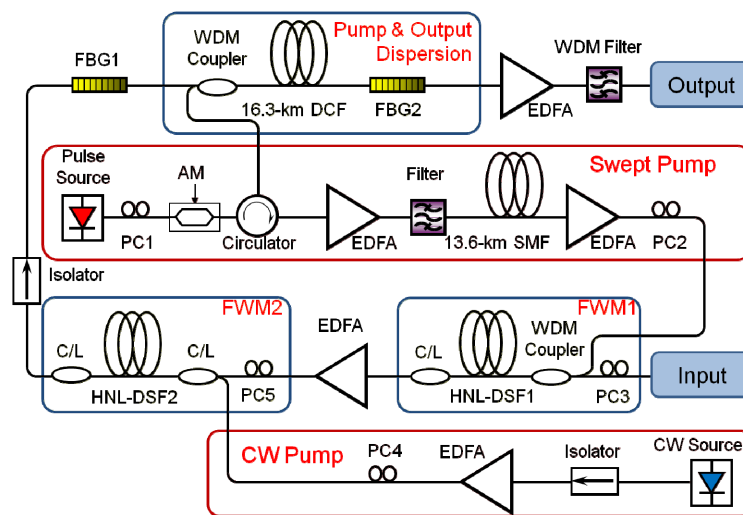

Fig. 2. Detailed experimental setup of PASTA system, pump stretching and output dispersion share the same spool of DCF. EDFA: erbium-doped fiber amplifier; FBG: fiber Bragg grating; AM: amplitude modulator; PC: polarization controller; C/L: C-band and L-band WDM coupler.

The output dispersion was the other essential part of the PASTA system, which was realized here by propagating through the same 16.3-km DCF to accomplish the time-lens focusing mechanism. Based on this configuration, we measured the pulse shapes of the PASTA system as shown in Fig. 4. From the stretched pump pulse (Fig. 4(a)), it can be observed that there were some high-frequency fringes on the stretched envelop of pump. These fringes were introduced in the frequency down-converted process, where the AM cannot fully suppress the 10-GHz neighboring pulses, and the residual pulses interfered with the passing one after the stretching process. These fringes were also transferred onto the newly generated idler, as shown in Fig. 4(b). At the output, all these features were compressed into short pulse, where the photodetector cannot resolve these fringes anyway, so these fringes would not affect the PASTA performance. The signal under test contained four equalized CW sources, roughly spaced by 1 nm from 1542 nm to 1545 nm, and the PASTA output trace is shown in Fig. 4(c). Three periods were shown here, which was reasonably stable. In Fig. 4(c), the temporal axis within each period can be converted into the corresponding wavelength axis by Eq. (9).
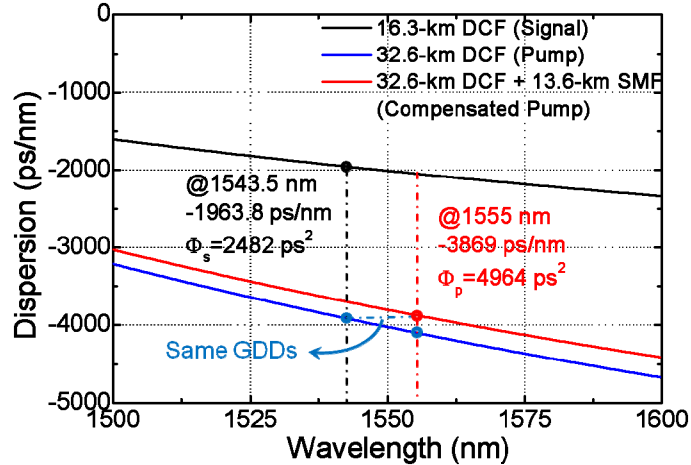
Fig. 3. Relation between the pump dispersion and the output dispersion at different wavelength. To ensure the pump stretching GDD is twice of the output GDD, the pump pulse should pass the same 16.3-km DCF twice. However, since the pump wavelength (1555 nm) had larger dispersion than the signal wavelength (1543.5 nm), another 13.6-km SMF was employed to compensate it.
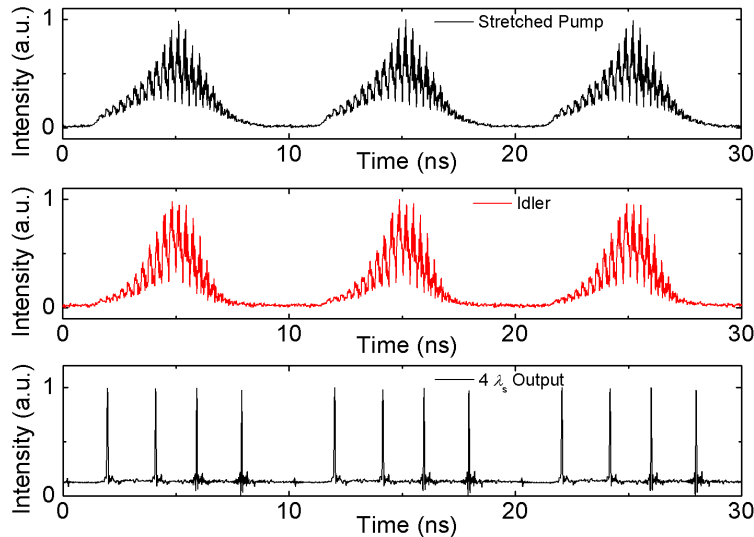

Fig. 4. The stationary performance of the PASTA system, with 100-MHz frame rate and four equally-spaced CW sources under test: (a) the stretched pump traces with the interference fringes; (b) the idler traces generated after the first-stage FWM; (c) four CW sources with different wavelength were captured by PASTA system.

4. Performance of the PASTA system

In addition to the stationary measurement shown above, PASTA system has also been demonstrated in resolving spectrum with ultrahigh frame rate (over 100 MHz) [19]. It is of great importance for the observation of some dynamic processes, such as the instantaneous linewidth of a swept-source [5,6], the spectrum evolution of a laser cavity during its stabilizing process [7,8], or some chemical dynamics [9]. However, when compared with standard spectroscopy, it can be observed that the intensity conversion was not uniform across the whole period, and higher-order dispersion also made the wavelength-to-time mapping relation nonlinear [22]. Therefore, some calibrations are required before its practical

implementation. In this section, we will present a thorough investigation on the PASTA performance, including the resolution, the wavelength range, the conversion efficiency, the power dynamic range and polarization sensitivity of this ultrafast wavelength resolving modality.

4.1. Resolution (Δλ)

The resolution reflects the capability of a spectroscopic system to distinguish different wavelengths. In PASTA system, according to the relation shown in Eq. (9), the wavelength resolution $\Delta\lambda$ is directly proportional to the temporal resolution Δt. Therefore, we first focus on the temporal resolution Δt that can be achieved. Equation (7) describes the intensity trace of the optical field, according to the mathematical relation: $\text{sinc}^2(0.4429) = 0.5$, we can obtain the full-width at half-maximum (FWHM) pulsewidth (temporal resolution):

$$\Delta t_o = 0.4429 \times 2 \times \frac{2\pi\Phi_f}{T} \tag{10}$$

However, in most cases, this optical pulsewidth is in picosecond range, which can hardly be captured without any distortion due to the limited detection bandwidth. Therefore, the practical electrical pulsewidth (temporal resolution) is:

$$\Delta t_e = t_{PW} = \frac{2\ln 2}{\pi f_{\text{BW}}}, \tag{11}$$

where the f_{BW} is the detection bandwidth. To fully resolve this optical pulsewidth ($\Delta t_e < \Delta t_o$), it is preferred to have larger detection bandwidth (f_{BW}), larger focal GDD (Φ_f), or smaller temporal aperture (T). Based on these two temporal resolutions, as well as the relation shown in Eq. (9), the wavelength resolution can be expressed by:

$$\Delta\lambda = \frac{\lambda_0^2}{2\pi c\Phi_f}\Delta t = \begin{cases} \dfrac{\lambda_0^2}{2\pi c\Phi_f}\Delta t_o = \dfrac{0.4429\times 2\lambda_0^2}{cT} & \text{(optical field limited)} \\[3mm] \dfrac{\lambda_0^2}{2\pi c\Phi_f}\Delta t_e = \dfrac{\lambda_0^2 \ln 2}{\pi^2 c\Phi_f f_{\text{BW}}} & \text{(electrical field limited)} \end{cases} \tag{12}$$
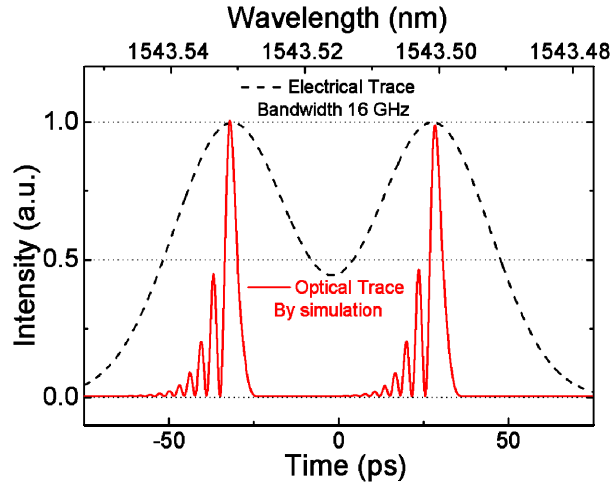

Fig. 5. Resolution performance of the PASTA system, with two close CW sources separated by 30 pm. The electrical trace was captured with 16-GHz electrical bandwidth (black dashed line), and compared with the simulated optical output pulse train (red solid line).

It can be deduced that, if the detection bandwidth is wide enough for the output pulse (optical field limited), the wavelength resolution is fully determined by the temporal aperture (T); while if the bandwidth is not wide enough (electrical field limited), the output pulse is broadened in the electrical domain, and it is primarily determined by the detection bandwidth and the focal GDD. In other words, larger bandwidth and larger focal GDD result in sharper wavelength resolution. For example, when the PASTA system is operated at the repetition rate of 100 MHz, it achieves the temporal aperture, $T = 3$ ns. Double passing the 16.3-km DCF, as well as the 13.1-km compensated SMF, resulted in the focal GDD, $\Phi_f = 1241$ ps^2. Therefore, if we only consider the optical field ($\Delta t_o = 4.6$ ps), the corresponding wavelength resolution is $\Delta\lambda = 2.34$ pm, without considering the high-order dispersion. In practical situation, the detection bandwidth (f_{BW}) was only 16 GHz, so $\Delta t_e = 27.6$ ps, and the electrical field limited resolution should be $\Delta\lambda = 14$ pm. Figure 5 shows the simulation result of the optical pulse train (red solid line) and the experimental captured electrical trace (black dashed line) of two CW sources separated by 30 pm, which is larger than the calculated ideal wavelength resolution (14 pm). From the simulated optical trace, it can be observed that there is a strong oscillation on the pulse leading edge, which is introduced by the aberration of the third-order dispersion from the time-lens part, and the interference of different spectral components produces a long tail of decaying oscillations [22,23]. Owing to the limited detection bandwidth, these high frequency fringes will be filtered out in the electrical trace, as the black dashed line shown in Fig. 5. Therefore, this aberration only slightly broadens the output pulses in the practical applications.
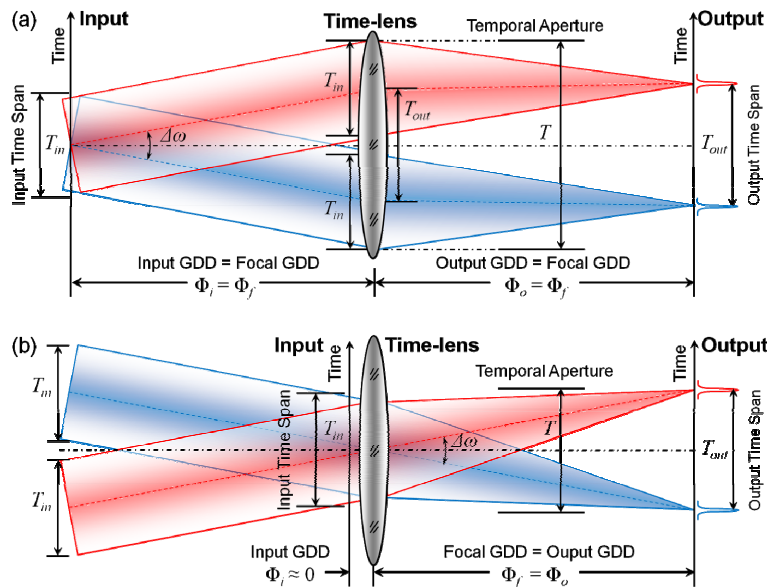
4.2. Wavelength range (λ_{BW})

Fig. 6. Two sets of time-lens focusing configurations in temporal ray diagram, with (a) or without (b) the input dispersion. The input GDD value affects the temporal aperture of the PASTA system.

Wavelength range of the spectroscopy reflects its converging ability, and it is also essential to quantify the PASTA capacity. According to the wavelength-to-time relation shown in Eq. (9), the wavelength range (λ_{BW}) is proportional to the output time span (T_{out}). To further clarify this relation, we first focus on the temporal aperture of the time-lens. In spatial optics, the paraxial approximation is a small-angle approximation of the light traveling through an axial optical system. Therefore, the pupil size (or aperture), an opening through which light travels, will significantly affect the imaging or focusing mechanism. For small pupil size, highly

collimated rays are admitted, so it results in a sharp focus on the image plane. While the large pupil size results in sharp image around where the lens is tightly focused, but blurred otherwise [16]. On the other hand, in the temporal imaging system, the temporal aperture not only requires the input signal fits within the effective range of the time-lens, it also requires to avoid overlapping between the neighboring periods, which is illustrated in Fig. 6.

Figure 6 exhibits two sets of time-lens focusing configurations, with (a) or without (b) the input dispersion. In configuration (a), two wavelengths are temporally separated by passing through the input dispersion; since the input GDD is equal to the focal GDD, these two diverged wavelengths are converted to the parallel transmission by the time-lens (shown as the dashed lines). While in configuration (b), these two overlapped wavelengths directly pass through time-lens; since the central wavelengths of these two fields intersect at the time-lens center (peak of the quadratic phase modulation), their directions are unchanged (shown as the dashed lines), though each single wavelength is focused after the output dispersion. Mathematically, these two configurations achieve the same output intensity trace, except with different phase terms. However, their temporal aperture requirements are also different. Here we define the input time span as T_{in}, and the output time span is T_{out}. In configuration (a), the input dispersion separates these two wavelengths by a time span of T_{out}, which exactly equals to the output time span. Therefore, at the time-lens, considering the input time span of T_{in}, the required temporal aperture should be $T = 2 \times (T_{in}/2) + T_{out}$. While in configuration (b), first, the time-lens is required to capture the input time span (T_{in}), and second, to make sure the output time span (T_{out}) is not overlapped with the neighboring periods, the time-lens period should be larger than T_{out}. Therefore, the overall temporal aperture is required to be $T = \max(T_{in}, T_{out})$. As a result, under the same temporal aperture (T), namely the same frame rate, configuration (b) can achieve larger output time span, especially when the output time span equals to the input time span ($T_{in} = T_{out} = T$). Therefore, the configuration (b) is applied in our PASTA system. According to Eq. (9), the PASTA wavelength range can be expressed as:

$$\lambda_{\mathrm{BW}} = \frac{\lambda_0^2}{2\pi c \Phi_f} T \tag{13}$$

Substituting the maximum $T = 10$ ns into Eq. (13), the theoretical wavelength range of our PASTA system is 5.16 nm, then the resolvable spectral points within one period is:

$$N_{eff} = \frac{\lambda_{\mathrm{BW}}}{\Delta\lambda} = \frac{T}{\Delta t_e} \tag{14}$$

where Δt_e is the pulsewidth of the electrical trace, and according to the theoretical calculation, $N_{eff} = 363$. In practice, 5-nm wavelength range (λ_{BW}) as well as 0.03-nm resolution resulted ($\Delta\lambda$) in $N_{eff} = 167$. Moreover, higher frame rate decreases the temporal aperture (T), e.g. if $T = 1$ ns, frame rate can be up to 1 GHz, which would result in worse resolution ($\Delta\lambda$) and narrower observation wavelength range (λ_{BW}). On the other hand, by decreasing the repetition rate (larger temporal aperture), larger non-overlapping wavelength range can be achieved. However, the maximum wavelength range is also limited by the phase matching condition of the FWM, since the spectral efficiency is non-uniform under wideband conversion (more discussion in section 4.3) [24]. Moreover, owing to the higher-order dispersion, the compensation between the pump dispersion and the output dispersion cannot cover a wide bandwidth. Distortion and broadening effects will be observed beyond the 5-nm wavelength range, though this can be improved with better dispersion engineered fiber.

4.3. Conversion efficiency of the parametric mixing

The implementation of time-lens is the most essential part in PASTA system; generally speaking, there are two major methods in achieving this quadratic phase modulation, the electro-optic phase modulator and the parametric mixing with linear chirped pump. The phase modulator is primarily applicable in high repetition rate (usually beyond 5 GHz), while the

parametric mixing with linear chirped pump could provide much larger chirped range and effective duty ratio under low repetition rate [23]. PASTA system is aimed at the frame rate from 10 MHz to 1 GHz, and requires larger effective time range. Therefore, the parametric mixing configuration is selected to implement the time-lens inside the PASTA system.

Highly-nonlinear dispersion-shifted fiber (HNL-DSF) is a promising medium to achieve this FWM based parametric mixing configuration, with high conversion efficiency. The entire process is shown in Fig. 7(a), after the first stage swept-source pumped FWM, double sweep range is imposed on the idler's side, as well as the conjugation of the input signal, which is shown as the negative sign in front of $\omega_s(t)$ term. Phase matching condition is essential in this wideband frequency conversion, and the gain only exists within the range satisfying $0 > \Delta k > 4\gamma P_0$, where Δk is the wave-vector mismatch [24]. Since the chirped idler is imposed with the quadratic phase modulation, the first stage FWM has already realized the time-lens function [25,26]. However, our PASTA system employs another phase conjugator – CW source pumped FWM to accomplish the time-lens. There are three advantages introduced by the second-stage FWM: (1) conjugated phase information of the signal is removed; (2) the chirped direction is opposite to that of the swept pump, then the output dispersion can employ the same dispersive fiber to compress the pulse; (3) the signal central wavelength is preserved, since the second-stage FWM pump wavelength is aligned with that of the first-stage FWM.
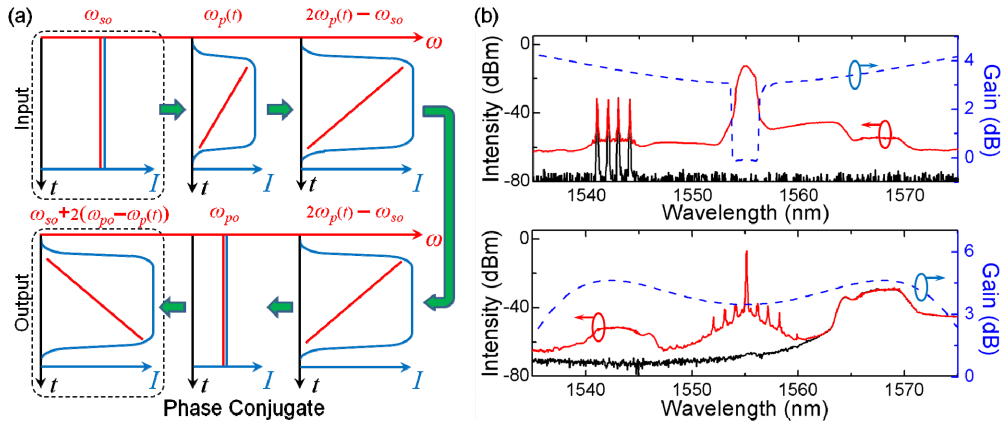

Fig. 7. Implementation of the time-lens by parametric mixing with linear chirped pump. (a) Mechanism of the two-stage FWM, a swept-source pumped FWM added with a CW source pumped FWM; (b) spectra of the two-stage FWM, as well as the wavelength conversion efficiency. The blue dash-dotted lines correspond to the gain spectra (right vertical axis).

The spectra of the first-stage FWM is shown in the top of Fig. 7(b), the wideband pump is not flat-top in spectrum, of which will be copied to the idler's side. While in the second-stage FWM, since the CW pump cannot be phase modulated to suppress the stimulated Brillouin scattering (SBS), it limits the CW pump power [27]; therefore, the conversion efficiency is relatively low, as shown in the bottom of Fig. 7(b).

4.4. Power saturation and polarization sensitivity

According to the PASTA output trace in Fig. 5, the peak power of each pulse corresponds to the intensity at each wavelength. Ideally, the PASTA peak power should be linearly proportional to the input power. However, owing to the gain saturation of the two-stage FWM, as well as the in-between booster amplifiers, the overall mapping is nonlinear. As the signal power increases, the amplifiers or FWM conversion may saturate, and output peak power will increase slowly. Therefore, the linear mapping of the spectral intensity only exists in the small-signal regime, and its mapping slope will decrease with higher signal power, as shown in Fig. 8(a). These constraints restrict the linear detection range from 1 µW (–30 dBm) to 100 µW, which corresponds to a linear dynamic range of 100. Lower power will be submerged into the amplified spontaneous emission (ASE) noise; while higher power can be

recalibrated by a power mapping curve as shown in Fig. 8(a), and up to 1-mW (0-dBm) power can be differentiated by calibration, i.e. the dynamic range of 1000.
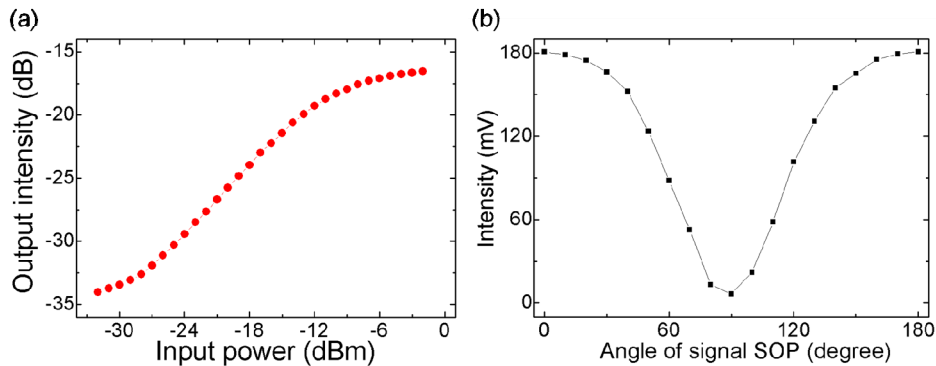

Fig. 8. Input conditions of the signal for the PASTA system. (a) The relation between the output intensity and the input power, in log-log scale. (b) Output intensity changed with the SOP of input signal, in linear scale.

In addition to the detection sensitivity, since FWM is a polarization-dependent process, the state of polarization (SOP) of the signal also affects the conversion efficiency. Monitored by a polarimeter, we changed the signal SOP by 180 degree with 10-degree steps, and the results are shown in Fig. 8(b). The FWHM of the output power corresponded to the signal SOP range from ± 60 degree. When the SOP was misaligned by 90 degree, the output power was almost fully suppressed. Therefore, adjustment of the SOP before detection is necessary for the PASTA system. It is noted that various techniques of achieving polarization-independent FWM have been demonstrated before [28].

5. Conclusion

PASTA system has been demonstrated as ultrafast spectroscopy by previous study. It precisely accumulates the same wavelength from an arbitrarily distributed time span into a single temporal point. Compared with the conventional OSA system, the PASTA system achieves orders of magnitude frame rate improvement, with comparable sensitivity and resolution performance. In this paper, we presented a thorough analysis on the performance of the PASTA system, including the resolution, the wavelength range, the conversion efficiency of the parametric mixing, the power saturation, and the polarization sensitivity. This analysis not only provides valuable insight into this new spectrum resolving system, but also serves as a design tool in optimizing a PASTA system. Ultrafast and single-shot operation of PASTA definitely provides a quick solution for many high-speed spectrum-resolving applications.